Broadband Quasielastic Scattering Spectroscopy Using a Multiline Frequency Comblike Spectrum in the Hard X-Ray Region

Makina Saito,[1,2,*] Masashi Kobayashi,[1,2] Haruki Nishino,[2,3] Toshiyuki Nishiyama Hiraki,[2] Yoshiaki Honjo,[2] Kazuo Kobayashi,[2,3] Yasumasa Joti,[2,3] Kyosuke Ozaki,[2] Yasuhiko Imai,[2,3] Mitsuhiro Yamaga,[2,3] Tetsuya Abe,[1,2] Nobumoto Nagasawa,[3] Yoshitaka Yoda,[3] Ryo Mashita,[4] Takaki Hatsui,[2] and Yusuke Wakabayashi[1]

[1]*Department of Physics, Tohoku University, Sendai, Miyagi, 980-8578, Japan*

[2]*RIKEN SPring-8 Center, 1-1-1 Kouto, Sayo, Hyogo, 679-5148, Japan*

[3]*Japan Synchrotron Radiation Research Institute (JASRI), 1-1-1, Kouto, Sayo, Hyogo, 679-5198, Japan*

[4]*Chemical Analysis Center, Sumitomo Rubber Industries Ltd., Kobe, Hyogo, 651-0071, Japan*

(Received 5 September 2023; revised 24 January 2024; accepted 19 April 2024; published 17 June 2024)

We developed a novel quasielastic scattering spectroscopy system that uses a multiline frequency comblike resolution function to overcome the limit on the accessible timescale imposed by the inherent single-energy resolution of conventional spectroscopy systems. The new multiline system possesses multiple resolutions and can efficiently cover a wide time range, from 100 ps to 100 ns, where x-ray-based dynamic measurement techniques are being actively developed. It enables visualization of the relaxation shape and wave-number-dependent dynamic behavior using a two-dimensional detector, as demonstrated for the natural polymer polybutadine without deuteration.

DOI: 10.1103/PhysRevLett.132.256901

Inelastic and quasielastic scattering techniques have been widely used to investigate the microscopic dynamics of selected structures in the wave number vector ($\boldsymbol{q}$) space. In the spectroscopic method using a monochromator and energy analyzer, the observed energy (E) spectrum is a convolution of the resolution function and dynamic structure factor $S(\boldsymbol{q}, E)$, which is the $\boldsymbol{q}$ and E domain representation of the Van Hove time space correlation function [1–3]. In quasielastic scattering experiments, the relaxation time of the structure characterized by $\boldsymbol{q}$ can be determined as $\sim\hbar/\Gamma$ by detecting the spectral broadening width Γ with respect to the width of the resolution function Γ_0, which is affected by the performance of both the monochromator and analyzer. At synchrotron radiation (SR) facilities, Si-backscattering monochromators and energy analyzers are used to achieve the $\Gamma_0 \sim 1$ meV resolution in inelastic x-ray scattering (IXS) spectrometers for studies of dynamics in picosecond timescale [1]. The SR with energy $E_0 = 14.4$ keV can be further monochromatized up to $\Gamma_0 \sim$ neV using a nuclear Bragg monochromator (NBM) based on the nuclear excitation-deexcitation phenomenon of the ^{57}Fe nucleus using the Mössbauer effect [4,5]. In this Letter, we refer to the radiation monochromatized by the nucleus as Mössbauer γ rays to distinguish it from other less monochromatic x rays [6]. It was shown that the radiation with $\Gamma_0 \sim$ several tens of neV is suitable for dynamics measurements at approximately 10 ns [7–9]. However, the higher the energy resolution Γ_0, the more limited the SR intensity used in the experiments. Therefore, the incident photon flux in 10-neV-resolution optics is typically 10^5 weaker than that in 1-meV-resolution optics. Extensive application studies have not been conducted because of flux limitations. In addition, the relaxation time is effectively determined typically when Γ/Γ_0 ranges from 0.1 to 10. The inherent limitations of conventional spectroscopic methods hinder effective broadband dynamic measurements.

In this Letter, we propose a novel spectroscopic method using a multiline frequency comblike structure of the Mössbauer γ-ray resolution function in the hard x-ray region. Based on the multiple resolutions and high flux, this novel system enabled effective broadband dynamic measurements compared to the conventional method. Optical frequency combs, in which spectral lines are distributed with well-defined splitting widths over a wide energy range, have been realized in the visible light range and extended to the extreme ultraviolet range [10–13]. The frequency comb structure facilitates broadband spectroscopic measurements, the realization of a precise optical clock, and the generation of arbitrary wave forms [10–13]. Efforts to extend the extreme ultraviolet range to the x-ray regime for obtaining broadband high-resolution x-ray frequency combs are ongoing [14]. In the hard x-ray region, the Mössbauer γ-ray emission-absorption from the nucleus naturally exhibits a multiline frequency comblike structure [15] when the nuclear energy levels are split by the Zeeman effect, as shown in Fig. 1(a), for the ^{57}Fe nucleus [4,16]. The number of lines, energy resolution, and splitting width (E_g and E_e for the ground and excited states, respectively) depend not only on the nucleus but also on the environment and can be artificially controlled [15–19].

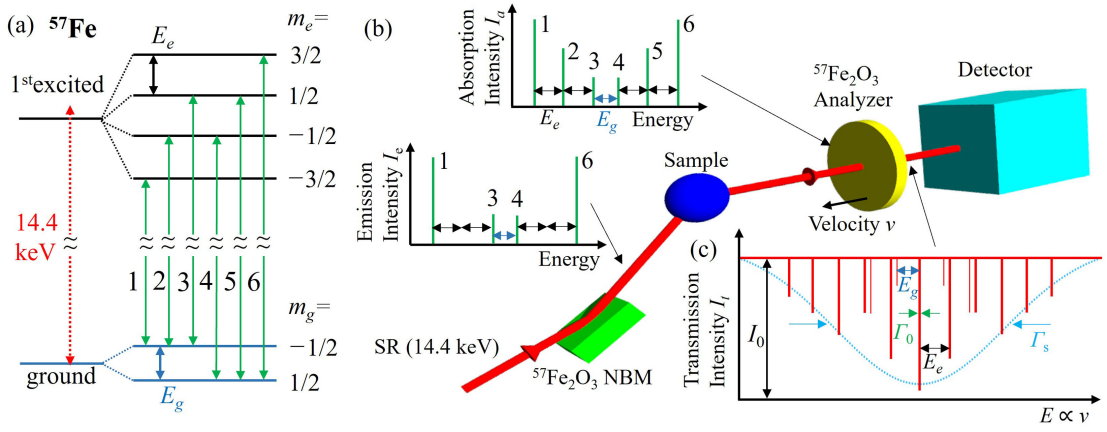

FIG. 1. ^{57}Fe nuclear energy levels and resulting multiline γ-ray spectra. (a) Magnetic hyperfine splitting of ^{57}Fe nuclear energy levels for the ground and first excited states. (b) Optics of the quasielastic scattering experiment using a $^{57}Fe_2O_3$ nuclear Bragg monochromator (NBM) and energy analyzer. The insets show schematics of the energy dependences of the Mössbauer γ-ray intensity emitted from the $^{57}Fe_2O_3$ NBM $I_e(E)$ and the absorption intensity of the $^{57}Fe_2O_3$ analyzer $I_a(E)$ neglecting the small effect of the quadrupole hyperfine interaction. (c) Transmission spectrum $I_t(E)$ detected at the detector position in the case of no dynamic effect.

Figure 1(b) shows a schematic of the proposed spectroscopy system using multiline γ rays to effectively examine the broadband dynamics. The system consists of a $^{57}Fe_2O_3$ NBM and a Mössbauer energy analyzer. The inset panels show the energy dependences of the multiline emission intensity $I_e(E)$ on the $^{57}Fe_2O_3$ NBM (bottom left) and the absorption intensity $I_a(E)$ on the $^{57}Fe_2O_3$ analyzer (top left) in the condition that the nuclear electric quadrupole hyperfine interaction is negligible. The energy of the multiline γ rays scattered by the sample was scanned using the analyzer, which masked the γ rays with energies corresponding to the absorption energy bands of the analyzer as in the Mössbauer spectroscopy. By applying velocity v to the analyzer, the absorption energy was shifted by $E = vE_0/c$ via the Doppler effect, where c denotes the speed of light. The absorption-type energy spectrum was obtained by measuring the transmitted intensity as a function of v (i.e., as a function of E). When there is no dynamic effect, the absorption profile of the transmission intensity is proportional to the convolution of $I_e(E)$ and $I_a(E)$, resulting in an absorption-type spectrum with a multiline frequency comblike structure consisting of 15 lines with a well-defined gap width, as shown in Fig. 1(c). The frequency comblike spectrum shown in Fig. 1(c) acts as the resolution function of a multiline system, in contrast to conventional energy-domain spectroscopic systems based only on a single-line component of the resolution function [7–9]. A dynamic effect appears in the absorption-type spectrum as a convolution of the multiline resolution function and $S(\boldsymbol{q}, E)$. We call the proposed method the multiline spectroscopy method of quasielastic γ-ray scattering (MLS QEGS). The multiline transmission spectrum shown in Fig. 1(c) exhibits the entire spectral width $\Gamma_s \sim 1.5$ μeV in addition to the basic resolution of each line $\Gamma_0 \sim$ several tens of neV. In the subsequent paragraphs, we demonstrate that the multiline structure allows us to obtain dynamic information on the energy scale of Γ_0 without largely sacrificing the intensity of the incident beam with spectral width Γ_s. The multiline spectrometer breaks the flux limitation imposed for single-line spectrometers. We also demonstrate the remarkably wide dynamic range of the MLS QEGS by simultaneously observing the broadening in both energy ranges of Γ_0 and Γ_s. The effectively measurable dynamic ranges of Γ/Γ_s and Γ/Γ_0 are 0.1–10, which correspond to broad timescales from sub-100 ps to several 100 ns in total, as shown in Fig. 2(a). Many groups are actively developing x-ray-based techniques to cover these timescales [20–25]. In addition, to maximize the performance of the MLS QEGS, we introduced the recently developed two-dimensional (2D) x-ray detector CITIUS, which enables effective measurements with a high q resolution and a sufficiently high frame rate to resolve each velocity in the velocity scan for obtaining the energy spectrum.

Figure 2(b) shows the experimental setup constructed at the nuclear resonant scattering hutch of BL35XU at SPring-8, Japan. The SR from the undulator was introduced into the $^{57}Fe_2O_3$ single-crystal NBM after passing through a Si(111) high-heat-load monochromator and a high-resolution channel-cut monochromator (6.5 meV resolution). The $^{57}Fe_2O_3$ NBM was placed in an external magnetic field of 900 G applied parallel to the incident SR's electric field polarization. The photon flux of the 14.4-keV γ ray from the $^{57}Fe_2O_3(111)$ plane was 5×10^6 counts/s. Scattered γ rays from the sample were introduced into a Mössbauer energy analyzer $^{57}Fe_2O_3$-powder plate (area density of 4 mg/cm^2 of ^{57}Fe). See Supplemental Material (SM), Sec. I for the energy spectrum of γ rays emitted by the NBM and the absorption spectrum of the analyzer plate [28]. The analyzer was

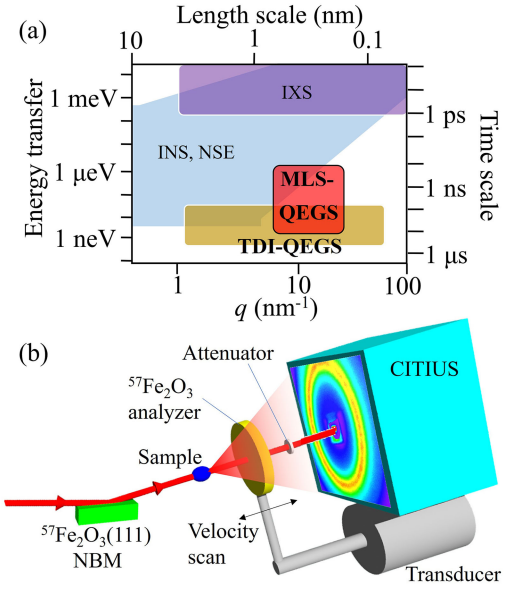

FIG. 2. (a) Length and timescales covered by some techniques. Those covered by inelastic x-ray scattering (IXS) [1], inelastic neutron scattering (INS) [2], and neutron spin echo (NSE) [3] are shown in addition to those covered by the multiline spectroscopy method of quasielastic γ-ray scattering (MLS QEGS) and time-domain interferometry (TDI) QEGS [26,27]. (b) Schematic of the experimental setup.

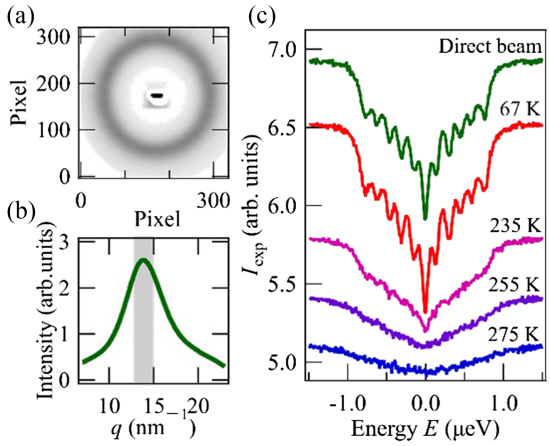

FIG. 3. Diffraction data and absorption-type quasielastic scattering spectra obtained for polybutadiene (PB). (a) Two-dimensional (2D) diffraction data and (b) q-dependent scattering intensity derived from the 2D diffraction data obtained for PB at 235 K. The highlighted region is the q region reflecting the interchain correlation, and the energy spectra were calculated to study the structural (α) relaxation time. (c) Absorption spectra of the direct beam and quasielastic scattering $I_{\mathrm{exp}}(q, E)$ obtained at $q = 14$ nm^{-1} [highlighted range in panel (b)] at 67, 235, 255, and 275 K from top to bottom.

driven by a voltage-velocity transducer (MVT-1000, Wissel) to modulate its absorption energy using the Doppler effect. We applied the sinusoidal velocity oscillation at a fixed period of 8.5 Hz with a maximum velocity of 30 mm/s, corresponding to the scanning energy range of ± 1.5 μeV, wide enough to observe all absorptions shown in Fig. 1(c). Using the same $^{57}Fe_2O_3$ material as the NBM and analyzer, the radiation and absorption energies were the same in all lines (Nos. 1, 3, 4, and 6) at velocity 0, where the elastic component was absorbed effectively. At v corresponding to other absorption peaks, the radiation and absorption energies coincided in one to three lines in the energy range of $\pm$sub1 μeV. The velocity was calibrated using a laser Doppler velocimeter (V100, Kyoritsu Electric Corp.).

QEGS is a photon-hungry technique. Therefore, it is desirable to provide q resolution using a 2D detector rather than the point detectors with a slit system used for conventional measurements, which discard most of the scattered intensity. Because the Doppler energy analyzer performs cyclic velocity scans that require time-resolved measurements, the detector should have a high frame rate, such as 8.5 kHz (1000 frames for one cycle of the analyzer's motion). Therefore, we introduced the CITIUS, a 2D x-ray detector with integrating-type pixels [30]. The CITIUS is equipped with 0.84 Mpixels with a pixel size of 72.6 μm square and is operated at 8.7 kHz, which is a sufficient frame rate for the MLS QEGS measurement. The thickness of the silicon sensor is 650 μm, with a nominal detection efficiency of 82% at a photon energy of 14.4 keV [31]. The CITIUS was placed in the forward direction, as shown in Fig. 2(b). The analyzer motion and exposure of the CITIUS were synchronized, as described previously [32]. By accumulating the count for each velocity point, we obtained the absorption-type quasielastic γ-ray scattering spectra as a function of the analyzer velocity at each pixel of the 2D diffraction data.

A standard polymer, polybutadiene (PB), was used to demonstrate the spectrometer's performance. Sample information is presented in Sec. II of SM [28]. The energy spectra were obtained at 67, 235, 255, and 275 K. The duration of the measurement was 2 h. The beam size at the sample position was 1 mm (horizontal) and 0.5 mm (vertical) in full width at half maximum. Figure 3(a) shows the 2D diffraction data for PB. The scattered γ rays were observed as rings, whereas the direct beam, which was transmitted through the sample and attenuator, was observed as an ellipsoidal spot in the central region. Because PB has an isotropic structure and dynamics, the q dependence of the scattered intensity was obtained by averaging the counts over the azimuthal angle, as shown in Fig. 3(b). The peak of the scattering intensity at $q \sim 14\,\mathrm{nm}^{-1}$ reflects the interchain structural correlation [33,34].

Although absorption-type quasielastic scattering spectra were obtained at many q simultaneously, we primarily focus on the data obtained at 14 nm^{-1} to demonstrate the structural (α) relaxation times as an example. The simultaneously obtained q-dependent relaxation times are described in Sec. III of SM [28]. A summation of each pixel's spectrum in the q region 14 ± 1 nm^{-1} was

computed considering the relative angle between the scattered γ rays and analyzer velocity for energy calibration. Figure 3(c) presents the data obtained at 67, 235, 255, and 275 K. We also show the spectrum of the direct beam transmitted through the sample, which exhibits a clear multiline structure. This direct beam spectrum is not affected by the sample dynamics and is treated as a resolution function. Among the expected 15 peaks, 11 well-separated peaks are visible in the spectra, where the energy scale of the quadrupole hyperfine interaction is smaller than Γ_0. The other four peaks shown as thin lines in Fig. 1(c) are fused with the neighboring peaks. The quasielastic scattering spectrum obtained at 67 K is almost identical to that of the direct beam, indicating that PB at 67 K is almost static. At 235 K, we observed the broadening of each fine peak, whereas the broadening of the entire spectrum was undetectable. In contrast, at 255 and 275 K, the multiline structures were completely smeared, and the broadening of the spectral distribution width Γ_s was observed. From the behaviors, the relaxation times ($\sim\hbar/\Gamma$) were found to be within an order of magnitude of $\hbar/\Gamma_0$ at 235 K and within an order of magnitude of $\hbar/\Gamma_s$ at 255 and 275 K. Thus, the two-step change in the spectrum was observed, as expected, as the timescale of the dynamics decreased with the heating of the sample. This behavior reflects the broadband nature of the novel system with multiple resolution functions, as discussed below.

The absorption profiles $I_A(q,E)$ were obtained to facilitate the analysis of the experimentally obtained spectrum $I_{\rm exp}(q,E)$ as $I_A(q,E)=[I_0-I_{\rm exp}(q,E)]/I_0$, where I_0 is a constant baseline value proportional to the incident γ-ray intensity. $I_A(q,E)$ is expressed as $I_A(q,E)=\int I_{\rm res}(E')S(q,E-E')\,dE'$, where $S(q,E)$ represents the normalized dynamic structure factor and $I_{\rm res}(E)$ represents the resolution function [35]. For $I_{\rm res}(E)$, we used the direct-beam spectrum $I_A(0,E)$ obtained simultaneously with the spectrum to be analyzed. An example of $I_{\rm res}(E)$ is shown in Fig. 4(a). To determine the shape of $S(q,E)$, we visualized the intermediate scattering function $F(q,t)$, the Fourier transform of $S(q,E)$, at 235 K, as shown in Fig. 4(b). Details of the evaluation are presented in Sec. IV in SM [28]. The relaxation of $F(q,t)$ was well reproduced by the Kohlrausch-Williams-Watts (KWW) function $f\exp[-(t/\tau)^\beta]$ with $\beta=0.45$ [33,34], where t, f, τ, and β denote the time, relaxation amplitude, relaxation time, and stretching exponent, respectively. All $I_A(q,E)$ were well fitted by assuming the Fourier transform of the KWW function with $\beta=0.45$ for the form of $S(q,E)$, as shown in Fig. 4(a) using the DAVE software from NIST [36].

The relaxation time τ was obtained by analyzing the spectra at 67, 235, 255, and 275 K. As expected, the relaxation time at 67 K, which is well below the glass transition temperature, was too long to be determined. This indicates that the spectrometer optics were stable during the experimental period, during which low-temperature

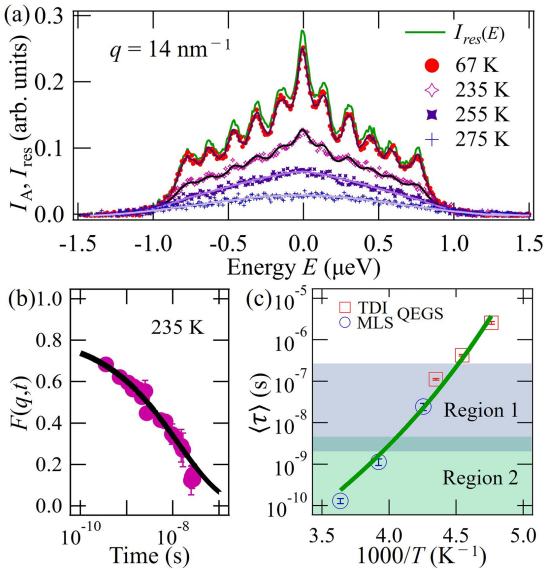

FIG. 4. Quasielastic scattering spectra and analysis results obtained for PB. (a) $I_{\rm res}(E)$ spectrum (direct-beam spectrum; most intense green curve) and $I_A(q,E)$ spectra obtained for PB at 67, 235, 255, and 275 K at $q=14$ nm^{-1}. The solid curves show the fitting curves. (b) Evaluated intermediate scattering function $F(q,t)$ for the spectrum obtained at 235 K (circles). The statistical error (standard deviation) was evaluated by the Monte Carlo error estimation [36]. The solid curve is the fitting curve by the Kohlrausch-Williams-Watts (KWW) function. (c) Temperature dependence of the obtained mean structural relaxation time $\langle\tau\rangle$ of PB. The $\langle\tau\rangle$ obtained at $q=14$ nm^{-1} by MLS QEGS (blue circles) and TDI QEGS (red squares) are plotted. The solid line is the fitting curve of $\langle\tau\rangle$ obtained by the Vogel-Fulcher-Tammann (VFT) law.

data can also be used for the resolution function [37]. In Fig. 4(c), the mean relaxation times $\langle\tau\rangle$ evaluated by $\langle\tau\rangle=\tau\Gamma(1/\beta)/\beta$ are shown as a function of temperature T with blue circles, where $\Gamma(x)$ is the gamma function [34]. $\langle\tau\rangle$ values at lower temperatures were also measured on the same sample at the same q using TDI QEGS [see Fig. 2(a)] [26,27]. The results are indicated by red squares. All the data follow the Vogel-Fulcher-Tammann (VFT) law $\langle\tau(T)\rangle\propto\exp\{DT_0/(T-T_0)\}$, which is widely used to analyze the temperature dependence of the α relaxation time, where D and T_0 are fitting parameters [34]. The fitting curve is shown as the solid curve in Fig. 4(c). The relaxation times obtained using the two techniques followed the single VFT law effectively and were consistent with the previous results [38], indicating the high accuracy of the present MLS QEGS measurements over a wide timescale of nearly 3 orders of magnitude.

In Fig. 4(c), the timescales expected to be effectively covered by the high-resolution Γ_0 and low-resolution Γ_s are shown as regions 1 and 2, respectively. It was confirmed that region 1 includes the relaxation time at 235 K, where the broadening of the fine peaks (with the resolution Γ_0)

was observed in Fig. 3(c). Region 2 includes the relaxation times obtained at 255 and 275 K, where the broadening of the entire spectrum (with the resolution Γ_s) was observed. Thus, we demonstrated that the multiline system covers a wide timescale of 100 ps to 100 ns owing to multiple resolutions. Furthermore, the incident beam flux was more than an order of magnitude higher than that obtained in previous single-line experiments performed in both energy ranges (Γ_s and Γ_0) because we avoided the flux loss caused by the generation of the single-line profile [9,24,25].

The multiple resolutions and high fluxes of the new system enable efficient broadband dynamic measurements. The complexity of the resolution function does not prevent us from observing the relaxation shape as we visualized the intermediate scattering function. The high flux allows for application studies where the scattering intensity is too weak to be studied using previous techniques, for example, at the off-peak of $S(q)$, as shown in Fig. S2 in SM [28]. Figure S2 also demonstrates that the q-dependent dynamic study was efficiently performed in a single experiment using a 2D detector. The new technique can potentially access q regions above $q = 20$ nm^{-1} that have not yet been fully explored at the nanosecond timescale, as shown in Fig. 2(a). Isotope substitution is not required for nanosecond structural dynamics studies of soft matter, as demonstrated for PB. This advantage significantly expands the range of target samples that can be studied at 100 ps–100 ns, which is an important timescale for various condensed matter sciences [39–46].

We are grateful to Professor Ko Mibu for allowing us to use their Mössbauer spectrometer and Dr. Takaya Mitsui (National Institutes for Quantum Science and Technology) and Dr. Alfred Q. R. Baron (RIKEN) for the insightful discussions. We thank the SPring-8 Accelerator Group for their assistance. The experiments were performed with the approval of the Japan Synchrotron Radiation Research Institute (2019A1442, 2020A0693, 2020A2038, 2021B1439, 2022A1343, and 2022B1293). This work was supported by JST-CREST (Grant No. JPMJCR2095), Japan, and the SACLA/SPring-8 Basic Development Program 2022–2023.

*Corresponding author: makina.saito.d6@tohoku.ac.jp

[1] A. Q. R. Baron, High-resolution inelastic x-ray scattering I: context, spectrometers, samples, and superconductors, in *Synchrotron Light Sources, and Free-Electron Lasers*, edited by E. Jaeschke, S. Khan, J. Schneider, and J. Hastings (Springer, Cham, 2015).
[2] S. W. Lovesey, *Theory of Neutron Scattering from Condensed Matter* (Clarendon Press, Oxford, 1984).
[3] D. Richter, M. Monkenbusch, A. Arbe, and J. Colmenero, *Neutron Spin Echo in Polymer Systems* (Springer, Berlin, 2005).
[4] R. Rohlsberger, *Nuclear Condensed Matter Physics with Synchrotron Radiation* (Springer, Berlin, 2005).
[5] G. V. Smirnov, V. V. Sklyarevskii, R. A. Voskanyan, and A. N. Artem'ev, ZhETF Pis. Red. **9**, 123 (1969).
[6] S. Yaroslavtsev and A. I. Chumakov, J. Synchrotron Radiat. **29**, 1329 (2022).
[7] D. C. Champeney and F. W. D. Woodhams, J. Phys. B **1**, 620 (1968).
[8] J. Z. Tischler, B. C. Larson, L. A. Boatner, E. E. Alp, and T. Mooney, J. Appl. Phys. **79**, 3686 (1996).
[9] R. Masuda, T. Mitsui, Y. Kobayashi, S. Higashitaniguchi, and M. Seto, Jpn. J. Appl. Phys. **48**, 120221 (2009).
[10] Th. Udem, R. Holzwarth, and T. W. Hänsch, Nature (London) **416**, 233 (2002).
[11] N. R. Newbury, Nat. Photonics **5**, 186 (2011).
[12] T. Fortier and E. Baumann, Commun. Phys. **2**, 153 (2019).
[13] N. Picqué and T. W. Hänsch, Nat. Photonics **13**, 146 (2019).
[14] S. M. Cavaletto, Z. Harman, C. Ott, C. Buth, T. Pfeifer, and C. H. Keitel, Nat. Photonics **8**, 520 (2014).
[15] G. Ramien, J. Gunst, X. Kong, and A. Pálffy, Phys. Rev. A **97**, 063858 (2018).
[16] N. N. Greenwood and T. C. Gibb, *Mössbauer Spectroscopy* (Chapman and Hall Ltd., London, 1971).
[17] S. L. Ruby and D. I. Bolef, Phys. Rev. Lett. **5**, 5 (1960).
[18] L. Pfeiffer, N. D. Heiman, and J. C. Walker, Phys. Rev. B **6**, 74 (1972).
[19] T. W. Sinor, O. Y. Nabas, J. D. Standifird, C. B. Collins, and E. Matthias, Phys. Rev. Lett. **66**, 1934 (1991).
[20] W. Roseker, S. O. Hruszkewycz, F. Lehmkühler, M. Walther, H. Schulte-Schrepping, S. Lee, T. Osaka, L. Strüder, R. Hartmann, M. Sikorski *et al.*, Nat. Commun. **9**, 1704 (2018).
[21] F. Lehmkühler, F. Dallari, A. Jain, M. Sikorski, J. Möller, L. Frenzel, I. Lokteva, G. Mills, M. Walther, H. Sinn *et al.*, Proc. Natl. Acad. Sci. U.S.A. **117**, 24110 (2020).
[22] Y. Sun, G. Carini, M. Chollet, F.-J. Decker, M. Dunne, P. Fuoss, S. O. Hruszkewycz, T. J. Lane, K. Nakahara, S. Nelson *et al.*, Phys. Rev. Lett. **127**, 058001 (2021).
[23] M. Reiser, A. Girelli, A. Ragulskaya, S. Das, S. Berkowicz, M. Bin, M. Ladd-Parada, M. Filianina, H.-F. Poggemann, N. Begam *et al.*, Nat. Commun. **13**, 5528 (2022).
[24] T. Mitsui, R. Masuda, M. Seto, and N. Hirao, J. Phys. Soc. Jpn. **87**, 093001 (2018).
[25] T. Mitsui, R. Masuda, S. Kitao, Y. Kobayashi, and M. Seto, J. Phys. Soc. Jpn. **91**, 064001 (2022).
[26] A. Q. R. Baron, H. Franz, A. Meyer, R. Rüffer, A. I. Chumakov, E. Burkel, and W. Petry, Phys. Rev. Lett. **79**, 2823 (1997).
[27] M. Saito, R. Masuda, Y. Yoda, and M. Seto, Sci. Rep. **7**, 12558 (2017).
[28] See Supplemental Material at http://link.aps.org/supplemental/10.1103/PhysRevLett.132.256901 for the description of NBM-emitted radiation spectrum and analyzer-absorption spectrum, sample information, and evaluation of intermediate scattering function, which includes Refs. [3,29].

[29] W. Knaak, F. Mezei, and B. Farago, Europhys. Lett. **7**, 529 (1988).
[30] T. Hatsui and H. Graafsma, IUCrJ **2**, 371 (2015).
[31] M. J. Berger, J. H. Hubbell, S. M. Seltzer, J. Chang, J. S. Coursey, R. Sukumar, D. S. Zucker, and K. Olsen, (2010), XCOM: Photon Cross Section Database (version 1.5). Available online: http://physics.nist.gov/xcom [2023, July 12]. National Institute of Standards and Technology, Gaithersburg, MD.
[32] H. Nishino *et al.*, Nucl. Instrum. Methods Phys. Res., Sect. A **1057**, 168710 (2023).
[33] D. Richter, B. Frick, and B. Farago, Phys. Rev. Lett. **61**, 2465 (1988).
[34] T. Kanaya, R. Inoue, M. Saito, M. Seto, and Y. Yoda, J. Chem. Phys. **140**, 144906 (2014).
[35] J. A. Elliott, H. E. Hall, and D. St. P. Burbury, Proc. Phys. Soc. **89**, 595 (1966).
[36] R. T. Azuah, L. R. Kneller, Y. Qiu, P. L. W. Tregenna-Piggott, C. M. Brown, J. R. D. Copley, and R. M. Dimeo, J. Res. Natl. Inst. Stand. Technol. **114**, 341 (2009).
[37] For the scattered γ rays, the effective thickness of the Doppler analyzer is increased because of the change in the incident angle. However, the effect is sufficiently negligible under current measurement conditions.
[38] A. Arbe, U. Buchenau, L. Willner, D. Richter, F. Farago, and J. Colmenero, Phys. Rev. Lett. **76**, 1872 (1996).
[39] M. Saito, S. Kitao, Y. Kobayashi, M. Kurokuzu, Y. Yoda, and M. Seto, Phys. Rev. Lett. **109**, 115705 (2012).
[40] T. Yamaguchi, M. Saito, K. Yoshida, T. Yamaguchi, Y. Yoda, and M. Seto, J. Phys. Chem. Lett. **9**, 298 (2018).
[41] M. Nagao, E. G. Kelley, A. Faraone, M. Saito, Y. Yoda, M. Kurokuzu, S. Takata, M. Seto, and P. D. Butler, Phys. Rev. Lett. **127**, 078102 (2021).
[42] R. Mashita, M. Saito, Y. Yoda, H. Kishimoto, M. Seto, and T. Kanaya, J. Synchrotron Radiat. **29**, 1180 (2022).
[43] P. Luo, Y. Zhai, P. Falus, V. G. Sakai, M. Hartl, M. Kofu, K. Nakajima, A. Faraone, and Y. Z., Nat. Commun. **13**, 2092 (2022).
[44] K. Mori, K. Enjuji, S. Murata, K. Shibata, Y. Kawakita, M. Yonemura, Y. Onodera, and T. Fukunaga, Phys. Rev. Appl. **4**, 054008 (2015).
[45] G. Schiró, Y. Fichou, F.-X. Gallat, K. Wood, F. Gabel, M. Moulin, M. Härtlein, M. Heyden, J.-P. Colletier, A. Orecchini, A. Paciaroni, J. Wuttke, D. J. Tobias, and M. Weik, Nat. Commun. **6**, 6490 (2015).
[46] C. L. Soles, A. B. Burns, K. Ito, E. Chan, J. Liu, A. F. Yee, and M. S. Tyagi, Macromolecules **53**, 6672 (2020).